

The properties of active galaxies at the extreme of eigenvector 1

M. Śniegowska^{1,2}, B. Czerny¹, B. You³, S. Panda¹, J.-M. Wang⁴, K. Hryniewicz³, and C. Wildy¹

¹ Center for Theoretical Physics, Polish Academy of Sciences, Al. Lotników 32/46, 02-668 Warsaw, Poland

² Warsaw University Observatory, Al. Ujazdowskie 4, 88-478 Warsaw, Poland

³ Copernicus Astronomical Center, Bartycka 18, 00-716 Warsaw, Poland

⁴ Key Laboratory for Particle Astrophysics, Institute of High Energy Physics, Chinese Academy of Sciences, 19B Yuquan Road, Beijing 100049, China

Preprint online version: January 16, 2017

ABSTRACT

Context. Eigenvector one is the formal parameter which allows to introduce some order in the properties of the unobscured type 1 active galaxies.

Aims. We aim at the understanding of the nature of this parameter, and with this purpose we analyze the most extreme examples of quasars with the highest possible values of the corresponding eigenvalues R_{Fe} .

Methods. We selected the appropriate sources from the SDSS and we perform a detailed modeling, including various templates for the Fe II pseudo-continuum and the starlight contribution to the spectrum.

Results. Out of 9 sources with the R_{Fe} larger than 2 selected from the SDSS quasar catalog only one quasar was confirmed to have a high value of R_{Fe} , equal 4.1. All other sources have R_{Fe} about 1. The high R_{Fe} object has an extremely narrow H β line, as in Seyfert 2 galaxies, but the [OIII] in this object is very weak in comparison with H β , the broad component of the line is present, with the width typical for a Narrow Line Seyfert galaxy.

Conclusions. Careful reanalysis of a larger sample from SDSS is needed to make stronger conclusions about the properties of the extreme eigenvector 1 sources.

Key words. Galaxies:active, Emission - radiative transfer, Accretion, accretion disks

1. Introduction

Active Galactic Nuclei (AGN) show a broad range of properties, when their emission lines and broad band spectra distributions are studied. Here we concentrate on the radio-quiet type 1 sources, but they also do not form a uniform sample, as expected in the simplest version of the AGN unification model (e.g. Peterson 1989). Theoretically, we still expect some dependence on the viewing angle, although in type 1 objects we have a clear view of the nucleus, on the black hole mass, Eddington ratio and the black hole spin. Observationally, Principal Component Analysis (PCA) showed that there is a hidden single parameter which correspond for the significant part of the dispersion in the measured parameters. This idea, first pointed out by Boroson & Green (1992), has been subsequently developed by numerous authors (e.g. Sulentic et al. 2000, Marziani et al. 2001; Kuraskiewicz et al. 2009; Shen & Ho 2014). Originally, the underlying Eigenvector 1 was a linear combination of several parameters. In recent years it was shown that the correlations are mostly driven by the ratio of the optical Fe II pseudo-continuum to the H β flux for sources where this spectral range is covered by the data.

However, the relation between the Eigenvector 1 and the theoretically motivated parameters is not yet quite clear. The Eddington ratio is most frequently favored (e.g. Sulentic et al.

2000), as already proposed by Boroson & Green in the original paper on that subject. Shen & Ho (2014) argued convincingly that the viewing angle is not involved, and it just provides a dispersion to the quasar main sequence. However, they did not solve uniquely the problem of the physical parameter varying along the quasar main sequence, as they showed that the Eddington ratio increases with Eigenvector 1 and the black hole mass decreases with Eigenvector 1.

We thus selected extreme sources populating Shen & Ho (2014) diagram. We selected sources with the measurement of Fe II optical flux and H β flux with accuracy better than 20%, and we reanalyze them much more carefully with the aim to confirm their extreme properties.

2. Method

2.1. Observational data

We select the extreme EV1 active galaxies from the Shen et al. (2011) catalog, taking into considerations only objects with the Fe II optical flux and H β measured with the error below 20%. We set the minimum value of the ratio R at 2.0, since the majority of the sources are at $R < 2.0$ (Shen & Ho 2011). In this way we selected 9 objects, the list is given in Table 1. The spectra were corrected for the Galactic reddening using the Cardelli et

Send offprint requests to: M. Śniegowska
marzena.sniegowska@student.uw.edu.pl

Table 1. Extreme EV1 objects selected for the study. Parameters taken from Shen et al. (2011) catalog.

| Name | RA | Dec | FWHM(H β) km s $^{-1}$ | R_{Fe} | EW(H β) Å | EW(FeII) Å | redshift | log L_{5100} | log M_{BH} |
|--------------------|---------|---------|----------------------------------|----------|---------------------|---------------|----------|----------------|--------------|
| 105234.19+233902.5 | 163.142 | 23.6507 | 3501.19 | 2.25271 | 37.66009 | 84.83739 | 0.4964 | 44.9492 | 8.47303 |
| 110036.57+064121.3 | 165.152 | 6.68926 | 1200.99 | 2.58476 | 15.04068 | 38.87657 | 0.2993 | 44.1789 | 7.15853 |
| 111123.80+505131.0 | 167.849 | 50.8586 | 3628.03 | 2.10273 | 36.35638 | 76.44781 | 0.5595 | 45.0336 | 8.54614 |
| 120950.85+554113.1 | 182.462 | 55.687 | 5299.09 | 2.34717 | 44.11553 | 103.5467 | 0.339 | 44.4972 | 8.607 |
| 125343.71+122721.5 | 193.432 | 12.456 | 8516.32 | 2.55857 | 74.69081 | 191.1018 | 0.2071 | 44.284 | 8.91249 |
| 131411.15+083759.8 | 198.546 | 8.6333 | 4499.46 | 2.12064 | 45.24653 | 95.95142 | 0.3589 | 44.4832 | 8.45793 |
| 141956.71+373912.8 | 214.986 | 37.6536 | 6143.18 | 3.00536 | 48.31863 | 145.2149 | 0.4768 | 44.7441 | 8.85883 |
| 150245.36+405437.2 | 225.689 | 40.9104 | 1202.69 | 2.11885 | 20.21656 | 42.83578 | 0.2329 | 44.1005 | 7.12057 |
| 165252.67+265001.9 | 253.219 | 26.8339 | 3345.21 | 2.56643 | 87.63021 | 224.8964 | 0.3501 | 44.937 | 8.42733 |

al. (1989) extinction curve and taking the required amount of reddening from NED¹.

We model the continuum emission of the selected AGN taking into account the contribution from the accretion disk as well as from the circumnuclear star cluster, and we model in detail the spectral region of the H β emission line. This is a complex multi-parameter task so we perform this fitting in a few separate steps.

2.2. Preliminary continuum fitting

We first use our own Fortran code to fit the continuum without the starlight. The emission lines are masked during the fitting, with 27 regions excluded (for the list of the masked regions, see Table 2). We model the disk emission assuming a power law shape, with the fix slope (i.e. the flux is modeled as $F_\lambda \propto \lambda^{-7/3}$) corresponding to the simplest model of an accretion disk (Shakura & Sunyaev 1973). We also test the possible effect of the curvature which is expected from the disk emission due to the presence of the maximum disk temperature, T_{max} , and in this case we model the disk spectrum as

$$F_\lambda \propto \lambda^{-7/3} \exp(-h\nu/kT_{max}), \quad (1)$$

where h is the Planck constant and k is the Boltzman constant.

The Fe II pseudo-continuum is modeled using the theoretical templates of Bruhweiler & Verner (2008). The templates are named as in Bruhweiler & Verner (2008), so the name specifies the local density, the ionization parameter and the turbulent velocity. The advantage of this approach over the observational templates is that the Fe II shape is well modeled also under the intense emission lines. On the other hand, the observational templates may also include other pseudo-continuum contributions like Fe III, while the theoretical templates are limited to Fe II itself. We thus generally use one of the theoretical templates (d11-m20-20; this is the template for the density 10^{11} cm $^{-3}$, ionization parameter 10^{20} cm $^{-2}$ s $^{-1}$ and the turbulent velocity of 20 km s $^{-1}$) but we also test other templates from the same set as well as observational template by Boroson et al. (2002) which was used by Shen et al. (2011). We also include the Balmer Component, described as in Dietrich et al. (2002) and the references therein. Blue-ward of the Balmer edge ($\lambda \approx 3675$ Å), we use the Planck function $B_\nu(T_e)$ (Grandi 1982) with constant electron temperature of 15 000 K. The optical depth change with wavelength is computed using a simple formula:

$$\tau_\nu = \tau_{BE} \left(\frac{\nu}{\nu_{BE}} \right)^{-3}, \quad (2)$$

where τ_{BE} is the optical depth at the Balmer edge radiation frequency (ν_{BE}). Red-ward of the Balmer edge blend of hydrogen emission lines is generated, using atomic data of Storey & Hummer (1995) with the recombination line intensities for case B (opaque nebula), $T_e = 15\,000$ K, $n_e = 10^8 - 10^{10}$ cm $^{-3}$. The accounted Balmer emission lines covered excitation top level for the transitions in the range $10 \leq n \leq 50$.

Fitting the continuum in this way we obtain the normalizations of the Fe II and BC pseudo-continua for each object.

2.3. Starlight fitting

We subtract the Fe II and BC pseudo-continua at the basis of the preliminary fits described above, and we model next the starlight contribution to the spectrum. We use the code STARLIGHT², described by Cid Fernandes et al. (2005,2009), in the version based on 45 stellar templates of Bruzual & Charlot (2003) corresponding to different stellar ages (15 options) and metallicities (3 options). The STARLIGHT allows also for a presence of a power law, and we fix again its slope at 7/3, as before, but the relative normalization is arbitrary. We use the same mask as in Sect. 2.2 in order to avoid the bands strongly contaminated by AGN emission lines. The code allows for stellar extinction. The code allows to obtain the relative contribution of 45 stellar components and of a power law through a Monte Carlo Markov Chain approach. The method minimizes the number of requested components. The code also returns the stellar velocity dispersion.

2.4. Emission line fitting

Next we concentrate on the wavelength region 4400 - 5100 Å where optical Fe II and H β are calculated. Since this range is relatively narrow we fix the relative normalization of the starlight to power law ratio and the stellar content as derived in Sect. 2.3 as well as the starlight reddening. However, we allow for the change of the overall normalization of the starlight plus Balmer Continuum plus a power law contribution. Fe II is treated separately, and its normalization is allowed again to vary. We now remove the use of the emission line mask and we model the line emission. In the case of some objects the STARLIGHT code did not indicate any power law contribution, so in this case we had to allow for the power law normalization to vary.

H β is modeled taking into account the decomposition into the broad and narrow component. Here we follow the approach of Shen et al. and tie the width of the narrow component of H β to [OIII] line, and both are represented as Gaussian lines. The broad component of H β is modeled either as a Gaussian or as

¹ NASA/IPAC Extragalactic Database

² <http://astro.ufsc.br/starlight/node/1>

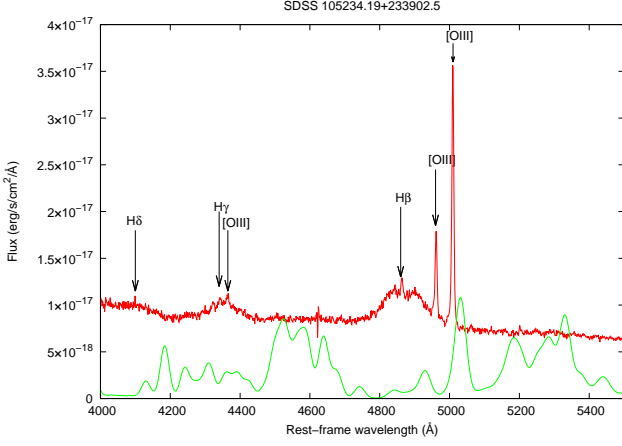


Fig. 1. The expanded region of the H β line of the source SDSS105234.19+233902.5 (red line) which does not show the presence of Fe II in our re-analysis; green line shows shape of the Fe II template d11-m20-20 broadened with a Gaussian of 900 km s⁻¹.

a Lorentzian component. We also include broad H γ in our fits since the tail of this line affect the spectrum close to 4400 Å.

[OIII] doublet is modeled assuming the theoretical ratio (1:3) between the strengths of the two components.

2.5. Determination of a new value of R_{Fe}

The normalization of the Fe II component is again allowed to vary at that stage of the fitting, and we use the same templates as during the preliminary fits (see Sect. 2.2). The equivalent width of the Fe II is calculated in the 4434 - 4684 Å range following the definition of Shen & Ho (2014). In both the case of Fe II and H β broad component we calculate the line EW with respect to the underlying power law, i.e. we do not include the starlight contribution. This is large modification in comparison with Shen et al. (2011) who do not differentiate between the accretion disk continuum and the starlight.

2.6. Results

Our analysis of the extreme EV1 sources show that the careful individual approach to fitting their spectra is indeed important and modifies the source parameters considerably.

2.7. Starlight contamination

Sources selected at the extreme tail of the EV1 have high Eddington ratios but at the same time they also have low values of the black hole masses (Shen & Ho 2014) so their nuclear luminosity is not always outshining the rest of the galaxy. The starlight contamination as determined from our data fitting ranges from 12.9 % up to 95.6 %. (see Table 3). The highest starlight contamination is in the source 150245.36+405437.2 which is notified for starburst activity in SDSS standard output³.

It is interesting to note that in general the stellar populations contaminating our sources consist of different stellar populations. In SDSS125343.71+122721.5 the population consists of a mixture of very young stars (1 Myr) and old stars (13.0 Gyr). Young stars are also present in SDSS105234.19+233902.5. In

Table 2. Masked regions during the preliminary continuum fitting (see Sect. 2.2) and with STARLIGHT fitting.

| No | λ_{min} [Å] | λ_{max} [Å] |
|----|------------------------|------------------------|
| 1 | 1000.0 | 1565.0 |
| 2 | 1620.0 | 1680.0 |
| 3 | 1880.0 | 1940.0 |
| 4 | 2290.0 | 2340.0 |
| 5 | 2390.0 | 2430.0 |
| 6 | 2640.0 | 2660.0 |
| 7 | 2780.0 | 2820.0 |
| 8 | 3120.0 | 3140.0 |
| 9 | 3160.0 | 3660.0 |
| 10 | 3720.0 | 3740.0 |
| 11 | 3850.0 | 3890.0 |
| 12 | 3960.0 | 3980.0 |
| 13 | 4080.0 | 4110.0 |
| 14 | 4320.0 | 4360.0 |
| 15 | 4670.0 | 4700.0 |
| 16 | 4830.0 | 4900.0 |
| 17 | 4940.0 | 4970.0 |
| 18 | 4990.0 | 5030.0 |
| 19 | 5400.0 | 5440.0 |
| 20 | 5840.0 | 5940.0 |
| 21 | 6280.0 | 6400.0 |
| 22 | 6500.0 | 6620.0 |
| 23 | 6700.0 | 6740.0 |
| 24 | 7040.0 | 7080.0 |
| 25 | 7840.0 | 7900.0 |
| 26 | 8440.0 | 8470.0 |
| 27 | 8830.0 | 9000.0 |

four objects an intermediate age stellar population dominated, with ages between 10 and 40 Myr, and those have relatively high contamination by the starlight. The velocity dispersion is typically around 200 km s⁻¹. The extinction in the starlight is not determined reliably since it is strongly coupled to the possible extinction towards the accretion disk which is neglected in the STARLIGHT code. However, this is not essential in the analysis of the H β line region.

2.8. H β properties

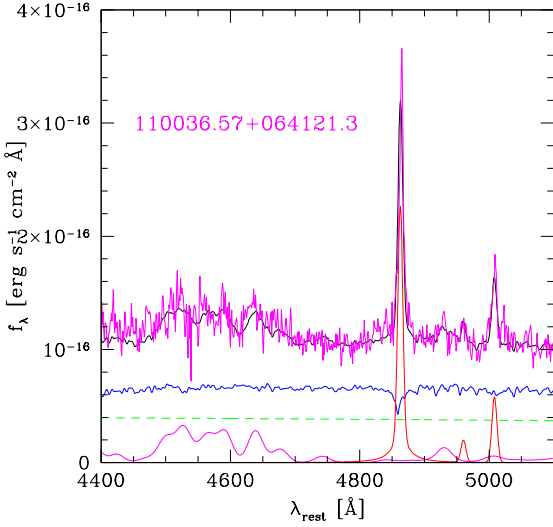
Gaussian shape appeared more suitable for some of the sources than the Lorentzian shape, consistently with the general knowledge that the Lorentzian shape is more suitable for the Narrow Line Seyfert galaxies (Laor et al. 1997). In our sample only two sources are from that class while the remaining 7 sources belong to the typical Seyfert 1 population. In the case of quasars the usual limit between type A and type B sources is at 4000 km s⁻¹ instead of 2000 km s⁻¹ but the selected sources are not of the class of distant bright quasars, with the 5100 Å monochromatic flux rather in the Seyfert galaxy class, below 10⁴⁵ erg s⁻¹.

Object 110036.57+064121.3 has very narrow H β line, and its kinematic width is consistent with the width of the narrow component of [OIII]. Intensity of the [OIII] line is low so the object meets the criterion [OIII]/H β > 3 (this ratio is below 0.5 in our fits), and the contribution of the disk emission is important so the source cannot be considered as a Seyfert 2 galaxy. The relative shift between [OIII] and H β is only 89.3 km s⁻¹, and the fit is marginally better if the additional H β component shifted by the same velocity is also present ($\Delta\chi^2 = 3.0$). The object is well fitted (see Fig. 2, with noticeable Fe II).

³ <http://skyserver.sdss.org>

Table 3. The properties of the extreme EV1 sources determined in our spectral analysis.

| Name | starlight at 4035 Å | EW (Fe II) | EW (H β) | R_{Fe} | FWHM(H β) |
|--------------------|------------------------|------------|-----------------|----------|------------------|
| | [%] | Å | Å | | km s $^{-1}$ |
| 105234.19+233902.5 | 25.0 | 0.0 | 63.2 | 0.0 | 2508 |
| 110036.57+064121.3 | 23.6 | 111.3 | 27.3 | 4.1 | 1862 |
| 111123.80+505131.0 | 12.9 | 102.0 | 98.2 | 1.0 | 2904 |
| 120950.85+554113.1 | 58.2 | 249.0 | 222.3 | 1.1 | 2194 |
| 125343.71+122721.5 | 49.7 | 84.3 | 65.0 | 1.3 | 1834 |
| 131411.15+083759.8 | 40.2 | 82.4 | 76.0 | 1.1 | 4532 |
| 141956.71+373912.8 | 65.3 | 52.1 | 49.3 | 1.1 | 5136 |
| 150245.36+405437.2 | 95.6 | 70.6 | 86.8 | 0.8 | 3498 |
| 165252.67+265001.9 | 49.0 | 70.2 | 86.9 | 0.8 | 2508 |


Fig. 2. The expanded region of the H β line of the source SDSS110036.57+064121.3 (red line) which shows extremely narrow line; green line shows shape of the Fe II template d11-5-m20-20-5-mod.dat broadened with a Gaussian of 700 km s $^{-1}$.

2.9. Extreme R_{Fe} objects

In most cases the value of the R_{Fe} derived from our analysis is smaller than originally derived by Shen & Ho (2014). However, in the case of one object we confirm very high ratio. This is the object showing the smallest H β width. The object is indeed extreme. The H β emission is strongly dominated by the narrow component, the broad component contains only 30 % of the narrow component flux. This is less than reported by Zhou et al. (2006) who gave similar values for both components. The kinematic width of the broad components is typical for Narrow line Seyfert 1 (NLS1) galaxies (see Table 3), the width of the narrow component is also rather normal ($FWHM = 472$ km s $^{-1}$). The black hole mass derived from our fits is $\log 7.48$, somewhat larger than measured by Shen et al. (2011). $EW(H\beta)$, if measured with respect to the absorbed power law is also quite typical (see Zhou et al. 2006), but the reddening of the power law component is large ($A_V = 1.31$), so if we measure H β with respect to uncorrected power law the line is extremely faint ($EW(H\beta) = 7.4$ Å). In such a case the source would have been classified as a Weak

Line Quasar (Wu et al. 2012). The reddening of course does not affect the measurement of the R_{Fe} .

3. Discussion

The analysis confirmed the existence of the extreme EV1 quasars, although only one out of nine studies sources are in this class. The selected object SDSS110036.57+064121.3 has the $R_{Fe} = 4$, the object belongs to the NLS1 class, and if the H β width is measured with respect to the unabsorbed power law contribution from an accretion disk, the source also qualifies as a Weak Line Quasar. Nevertheless, the Fe II emission is relatively strong. The luminosity to the Eddington luminosity ratio in this source is not very high, 0.27, which may imply that the Eddington ratio itself is not the lonely driver of the Eigenvector 1. High Eddington ratio sources monitored by Du et al. (2016) occupy the region between $R_{Fe} = 0.5$ to $R_{Fe} = 1.9$ (P. Du, private communication).

We propose that the Eigenvector 1 is driven not just by the Eddington ratio but by the position of the maximum of the broad band quasar spectrum. This peak in turn, in the case of the simplest accretion disk model (Shakura & Sunyaev 1973) this maximum is connected with the maximum of the accretion disk temperature, and it scales with the black hole mass and accretion rate as

$$\nu_{max} \propto \left(\frac{\dot{M}}{M_{BH}}\right)^{1/4}, \quad (3)$$

i.e. $\nu_{max} \propto (\dot{m}/M_{BH}^2)^{1/4}$ (Tripp et al. 1994). The accretion rate is related to the bolometric luminosity, and the bolometric luminosity is usually estimated from the L_{5100} luminosity. The black hole mass in turn is determined again from the L_{5100} luminosity, and from the FWHM of the line. When the two are combined, the dependence on the luminosity vanishes, and we obtain a simple relation

$$\nu_{max} \propto FWHM^{-1}. \quad (4)$$

If our hypothesis is correct, the value R_{Fe} should only be connected with the value of FWHM of H β . In our list only one source has high R_{Fe} , but two sources have low values of FWHM. However, the two objects widely differ in actual line shape. In SDSS 110036.57+064121.3 the narrow component strongly dominates, and the overall line is very narrow, much narrower than the value of FWHM given in the Table 3 and corresponding only to the broad component. In SDSS 125343.71+122721.5 the broad component dominates. If indeed the whole line profile should be taken into consideration, the correlation of R_{Fe} with FWHM would indeed be very strong. Studies of more sources

may give some indication about the appropriate approach. In addition, this discussion does not take into account the influence of the viewing angle to the source which also can cause the appearance of very narrow lines simply due to the purely geometrical approach.

Our analysis takes into account the Fe II contamination much more carefully than the analysis done by Shen et al. (2011), and accounts for the starlight. However, we cannot achieve fully self-consistent fits yet. The STARLIGHT code does not allow to include the reddening to the power law or the effects of the maximum of the disk temperature, i.e. the flattening of the power law at shorter wavelengths.

Acknowledgements. The project was partially supported by Polish grant No. 2015/17/B/ST9/03436/. The STARLIGHT project is supported by the Brazilian agencies CNPq, CAPES and FAPESP and by the France-Brazil CAPES/Cofecub program. The Fe II theoretical templates described in Bruhweiler & Verner (2008) were downloaded from the web page <http://iacs.cua.edu/personnel/personal-verner-feii.cfm> with the permission of the authors. This research has made use of the NASA/IPAC Extragalactic Database (NED) which is operated by the Jet Propulsion Laboratory, California Institute of Technology, under contract with the National Aeronautics and Space Administration.

References

- Boroson, T. A., Green, R. F., 1992, *ApJS*, 80, 109
 Boroson, T. A., 2002, *ApJ*, 565, 78
 Bruhweiler, F., & Verner, E., 2008, *ApJ*, 675, 83
 Bruzual G., Charlot S., 2003, *MNRAS*, 344, 1000
 Cardelli, J. A., Clayton, G. C., Mathis, J. S., 1989, *ApJ*, 345, 245
 Cid Fernandes, R., Schoenell, W., Gomes, J. M., Asari, N. V., Schlickmann, M. et al., 2009, *RMxAC*, 35, 127
 Cid Fernandes R., Mateus A., Sodre L., Stasinska G., Gomes J., 2005, *MNRAS*, 358, 363
 Cid Fernandes, R., Storchi-Bergman, T., Schmitt, H.R., 1998, *MNRAS*, 297, 579
 Dietrich, M., Hamann, F., Shields, J. C., Constantin, A., Vestergaard, M. et al., 2002, *ApJ*, 581, 912
 Grandi, S. A., 1982, *ApJ*, 255, 25
 Kuraszkiewicz, J., Wilkes, B. J., Schmidt, G., Smith, P.S., Cutri, R., Czerny, B., 2009, *ApJ*, 692, 1180
 Laor, A. et al., 1997, *ApJ*, 489, 656
 Marziani, P., Sulentic, J.W., Zwitter, T., Dultzin-Hacyan, D., Calvani, M., 2001, *ApJ*, 558, 553
 Peterson, B. M., 1989, *An introduction to Active Galactic Nuclei*, CUP
 Shakura, N.I., & Sunyaev, R.A., 1973, *A&A*, 24, 337
 Shen, Y. et al., 2011, *ApJS*, 194, 45
 Shen, Y., Ho, L. C., 2014, *natur*, 513, 210
 Storey, P. J., Hummer, D. G., 1995, *MNRAS*, 272, 41
 Sulentic, J. W., Bachev, R., Marziani, P., Negrete, A. A., Dultzin, D., 2007, *ApJ*, 666, 757
 Sulentic, J.W., Zwitter, T., Marziani, P., Dultzin-Hacyan, D., 2000, 536, L5
 Tripp, T. M., Bechtold, J., Green, R. F., 1994, *ApJ*, 433, 533
 Wu, J. et al., 2012, *ApJ*, 747, 10
 Zhou, H., Wang, T., Yuan, W. et al., 2006, *ApJ*, 166, 128